Quantitative ultrasound imaging of roughness

Application to bone health assessment

Salomé VIGNAT

Supervised by Quentin GRIMAL and Amadou DIA

Laboratoire d'Imagerie Biomédicale

GRENOBLE INP UGA Phelma

Context of the study

The medical context

Osteoporosis: bone disease responsible of **37 millions fractures** in people aged 55 and above *[www.osteoporosis.foundation]*

➡ Caused by **increased porosity**

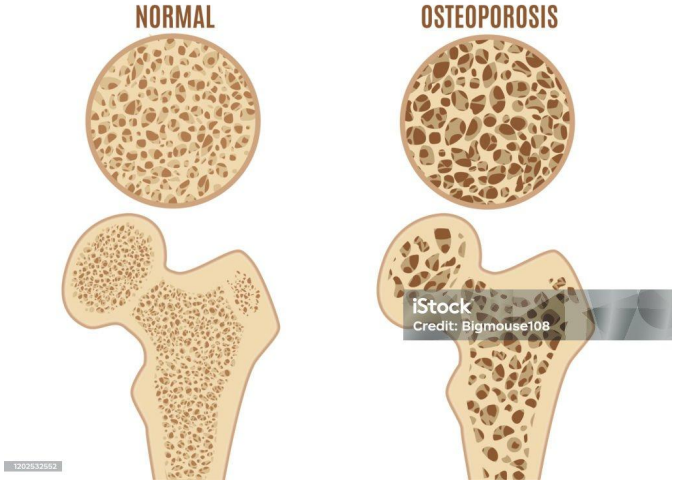

Fig 1 - Healthy and osteoporotic bones

Reference method for diagnosis:

Bone mineral density, evaluated with **Dual Energy X-Ray Absorptiometry**

BUT 60-70% of fractures happened to patient with a normal BMD

➡ This method is **limited**

[Schini et al. 2024n An overview of the use of the fracture risk assessment tool (FRAX) in osteoporosis]

Use of **ultrasound** (mechanical waves) to evaluate the **mechanicals properties** of the bone

Context of the study

Ultrasound imaging of the bone

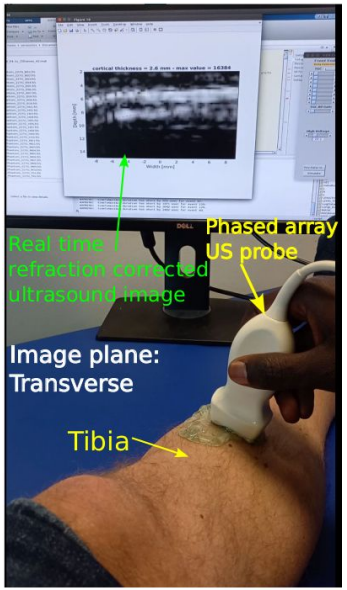

Fig 1 - Configuration for acquisition of ultrasound data

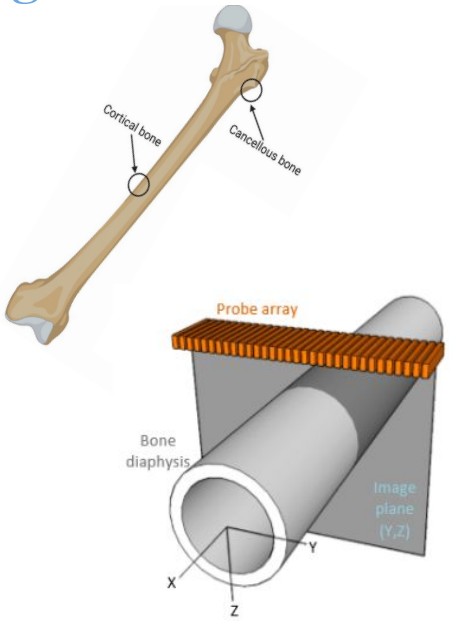

Fig 2 - Relative position of the ultrasound probe relatively to the bone

[Ma, Qianli et al. "Significance of mechanical loading in bone fracture healing, bone regeneration, and vascularization.]
[Renaud G, Kruizinga P, Cassereau D, Laugier P. In vivo ultrasound imaging of the bone cortex. Phys Med]

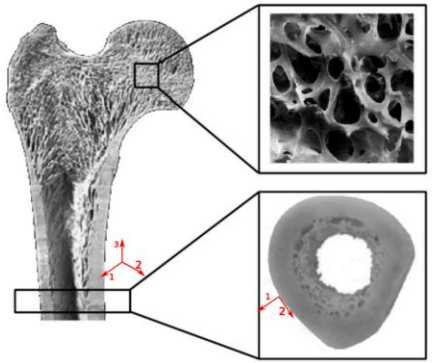

Fig 3 - Relative position of the ultrasound probe relatively to the bone

[Mathilde Mouchet. "Evaluation multi-échelle de la qualité osseuse par ultrasons". Thèse de doctorat dirigée par Laugier, Pascal Acoustique Physique Paris 7 2012.]

Bone thickness

Speed of sound in the bone

Laboratoire d'Imagerie Biomédicale

Context of the study

A method used in the detection of osteoporosis

Osteoporosis - bone disease modifying the microstructure and weakening the bone

➔ The **bone** is constantly **remodeling**

➔ **Imbalance** of the formation/resorption process

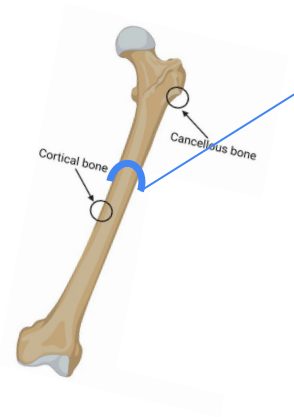

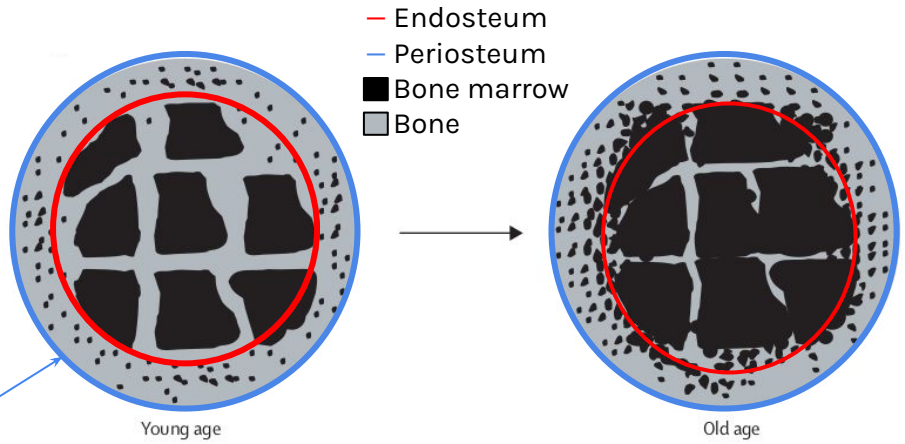

Fig 4 - Age-related bone loss and remodelling

[Zebaze, (2010). Intracortical remodelling and porosity in the distal radius and post-mortem femurs of women: A cross-sectional study.]

Context of the study

Find an additional biomarker

Transitional zone

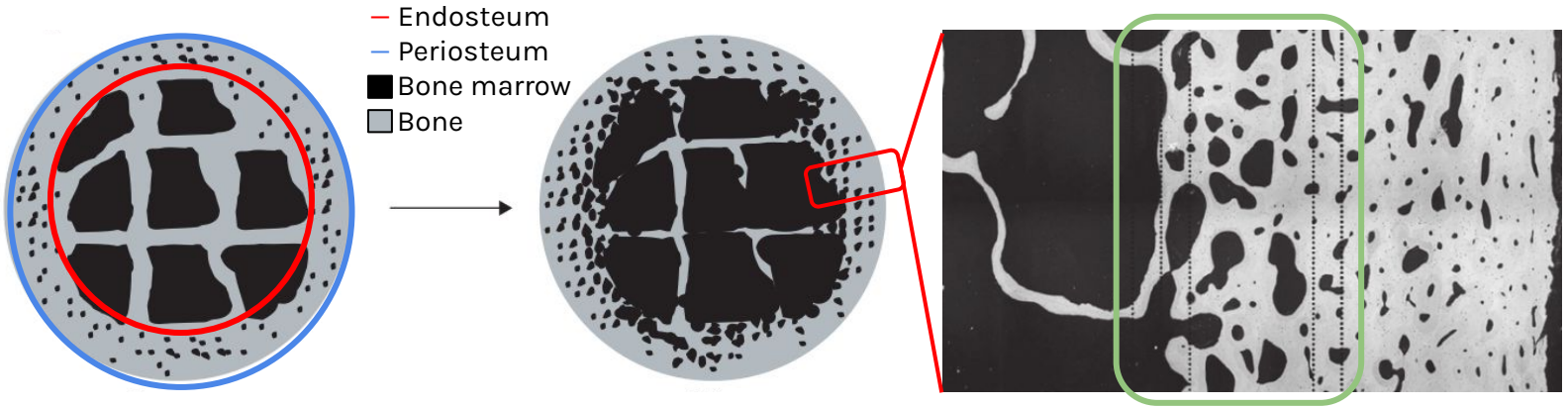

Fig 5 - Bone profile and pores repartition
[Zebaze, Transitional and Trabecular Compartments and Quantification of Cortical Porosity from High Resolution Peripheral Quantitative Computed Tomographic Images.]

➔ At **high biological activity** location, in the bone marrow
⇒ At the **endosteal interface**

⇒ Find additional biomarker to detect osteoporosis by quantitative ultrasound imaging

Context of the study

A proof of concept In Vivo

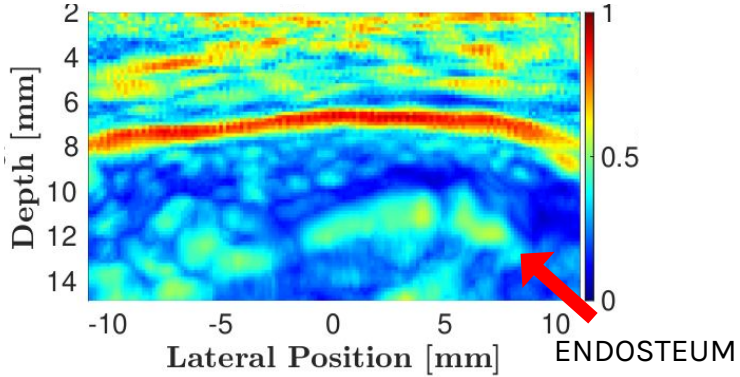

Fig 6 - Index of specularity on ***In-Vivo*** *bone*

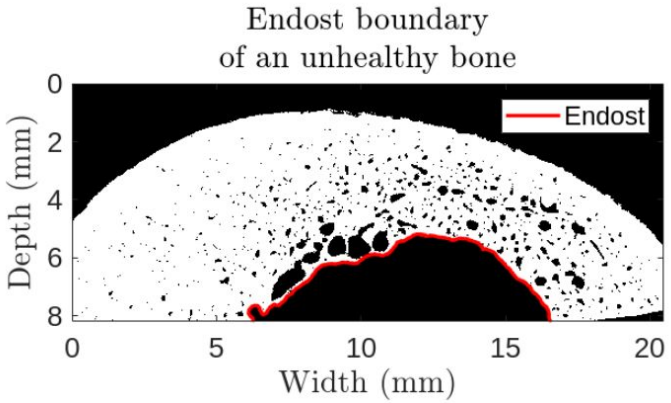

Fig 7 - ***Ex-Vivo*** *bone profile*

⚠️ *Not the same bone*

→ Ultrasounds react differently on smooth and rough surfaces

→ **Quantify and interpret this differency**

Context of the study

The basis of ultrasound imaging

PROBE PARAMETERS

Elements →transducers that emits and receipts mechanical waves with vibration.

Linear array → 96-elements array

Synthetic aperture → One element emitting, all element receptive.

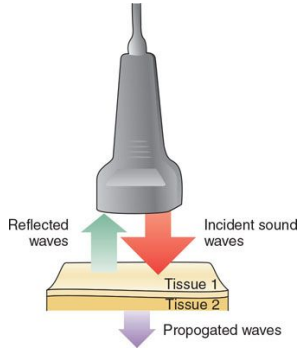

Fig 8 - Ultrasound transmission and reflexion on tissues.

[Image from RadiologyKey url: https://radiologykey.com/physics-of-ultrasound-2/]

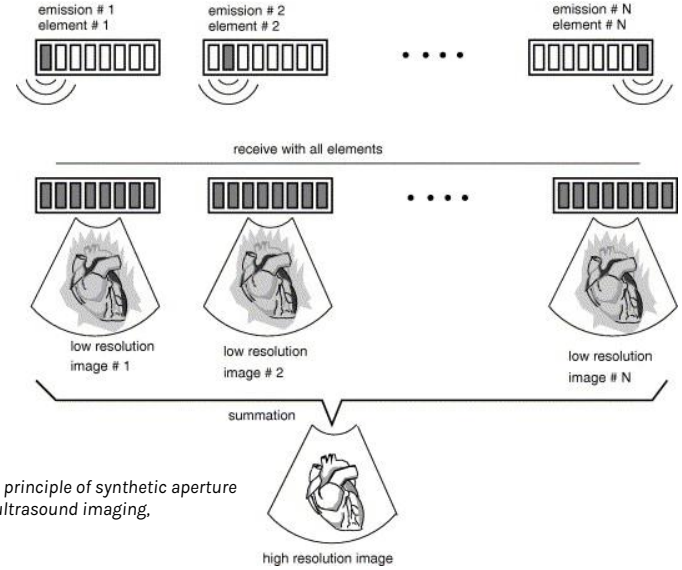

Fig 9 - Basic principle of synthetic aperture ultrasound imaging,

[Ihor Trots et al. "Synthetic Aperture Method in Ultrasound Imaging". In: Apr. 2011. isbn: 978-953-307-239-5. doi: 10.5772/15986]

Laboratoire d'Imagerie Biomédicale

Context of the study

The particularities of bone imaging

Delay-and-Sum beamforming

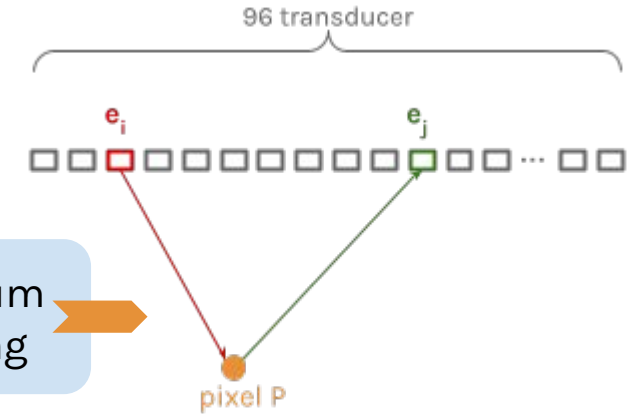

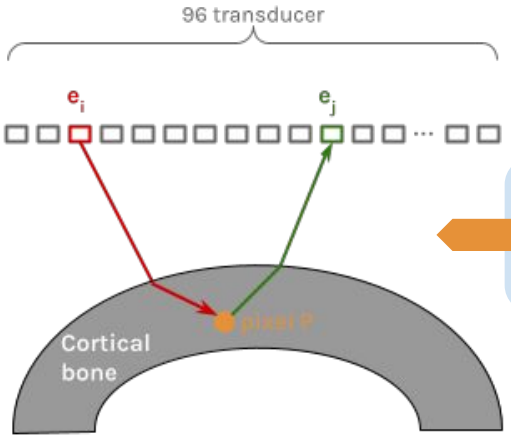

Bone imaging beamforming

Fig 10 - Ray path between elements and pixel

PIXEL RECONSTRUCTION

Intensity of the pixel = amplitude of the signal for a *receptor j* at $T_{i,j}$ that corresponds to the travel time between *emitter i* and *receptor j*

BONE IMAGING

Consider the **refraction** at the segmented outer surface of the bone.

Context of the study

Definition of a specular reflection

Acoustic waves react differently on specular and diffuse object

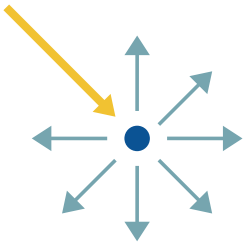

diffuse reflection

λ >> a

specular reflection

λ << a

a = characteristic size

λ = wavelength

The signal recorded by the ultrasound probe is different

Fig 11 - Reflection on diffuse and specular objects

PROBE

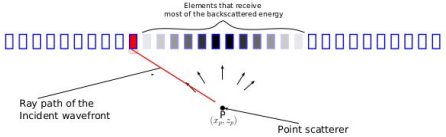

PROBE

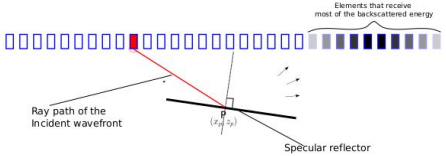

Fig 12 - Receiving element for different objects

[Amadou Dia. "Quantitative ultrasound imaging of human cortical bone". Thèse de doctorat dirigée par Quentin GRIMAL et Guillaume RENAUD. PhD thesis. 2024, 1 vol. (167 p.)]

Laboratoire d'Imagerie Biomédicale

Context of the study

Implemented method

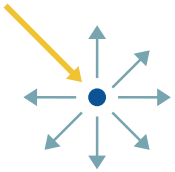

diffuse object
λ >> a

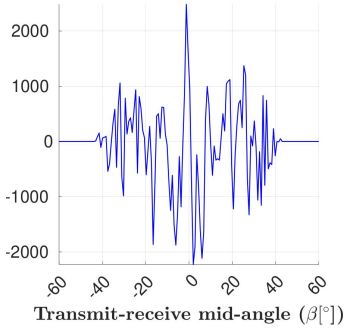

specular object
λ << a

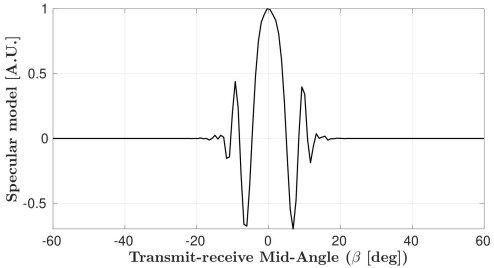

Fig 13 - Signal of a diffuse and a specular object

[Amadou Dia. "Quantitative ultrasound imaging of human cortical bone". Thèse de doctorat dirigée par Quentin GRIMAL et Guillaume RENAUD. PhD thesis. 2024, 1 vol. (167 p.)]

Normalized correlation in each pixel between a **signal of a perfectly specular object** and the **received signal**
⇒ **Index of specularity of the pixel Ψ**

Index = 1 ⇒ Specular surface
Index = 0 ⇒ Diffuse surface

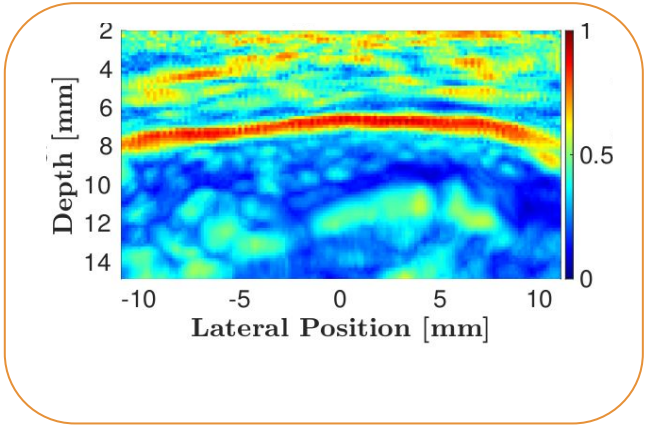

LIB10
Laboratoire d'Imagerie Biomédicale

Methodology of the research

How does the specular index Ψ behave regarding the bone microstructure ?

- **Parametric study** of the bone endosteum on *ex-vivo* bone images
- **Generation of interfaces** with different values of the defined parameters
- **Simulation** of the ultrasound propagation to understand the **influences of the defined parameters on the index Ψ**

Bone microstructure characterization

Parametric study of Bone Health Indicators

What parameters describe the bone microstructure ?

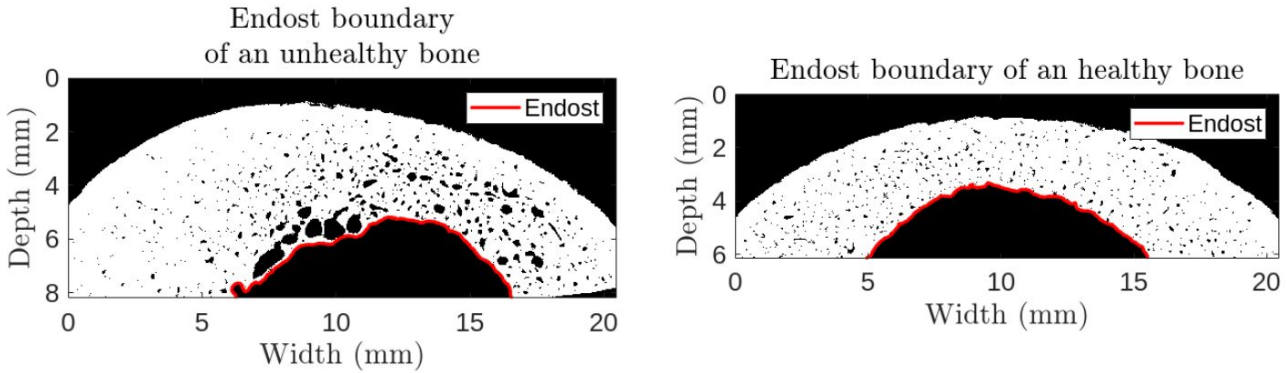

Fig 14 - Healthy (left) and unhealthy (right) bones

Bone microstructure characterization

Description of the bone surface, the endosteum

The parameters were determined by **image processing on *ex-vivo* bone**

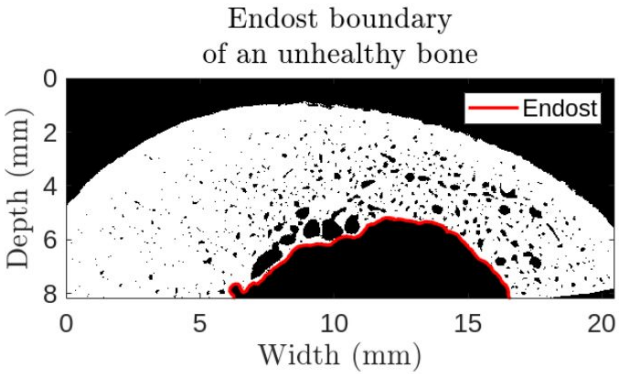

Fig 16 - Endosteal interface from the ex-vivo bone image

Images obtain with micro-CT with a 9µm resolution

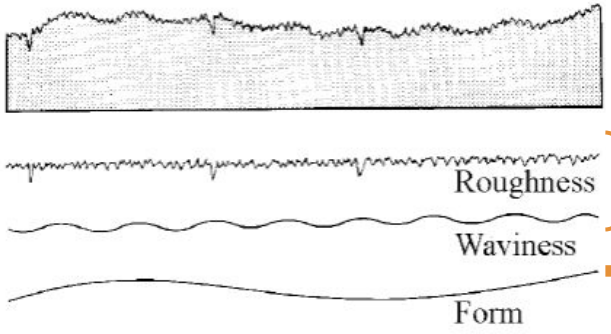

Fig 15 - Component of a surface

[Peter Ettl, Berthold E. Schmidt, M. Schenk, Ildiko Laszlo, Gerd Haeusler, Roughness parameters and surface deformation measured by coherence radar]

Informations we want to extract

Parabolic form of the bone we want to filter

High pass filter to obtain the desired profile

Bone microstructure characterization

Description of the bone surface, the endosteum

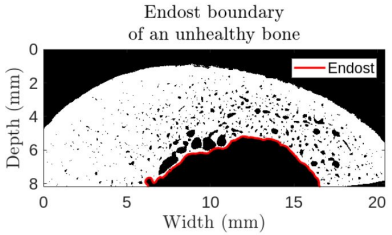

Choice of the **cut-off frequency** with the **mean height** of the profile

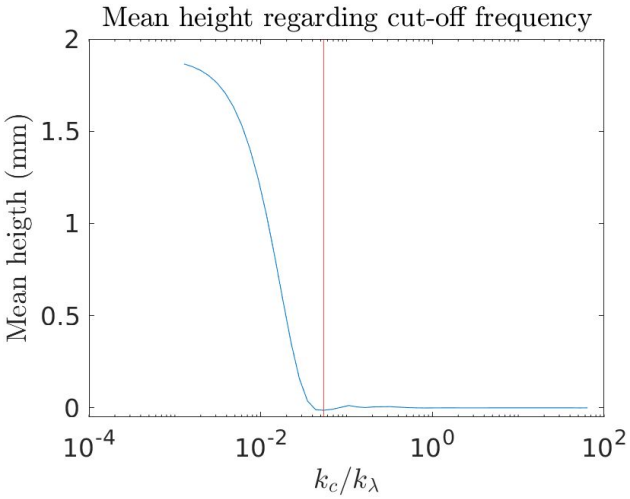

Fig 17 - Value of the cut-off frequency regarding the frequency in the bone

The cut-off frequency is
$k_c = 0.06 * k_\lambda = 0.043\ mm^{-1}$

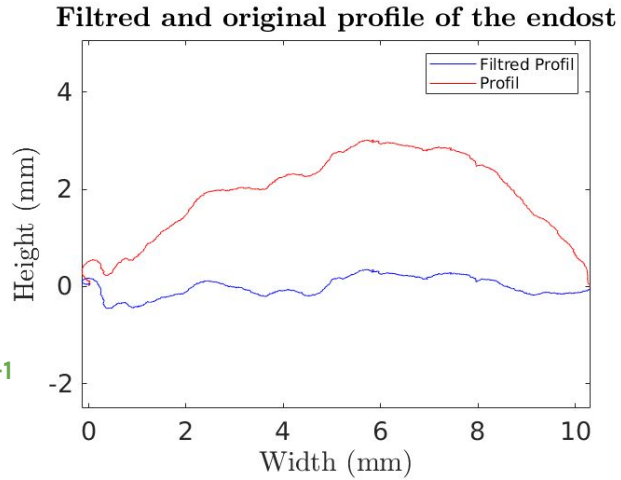

Fig 18 - Segmented profile and filtered endosteal profile

Wavelength in the bone $\lambda \approx 1.28\ mm$

Spatial frequency of the ultrasound wavelength in the bone $k_\lambda = 1/\lambda = 0.78\ mm^{-1}$

Bone microstructure characterization

The correlation length and the height root mean square

Profile regarding the height root-mean-square (Rq) and correlation length (ρ_{length})

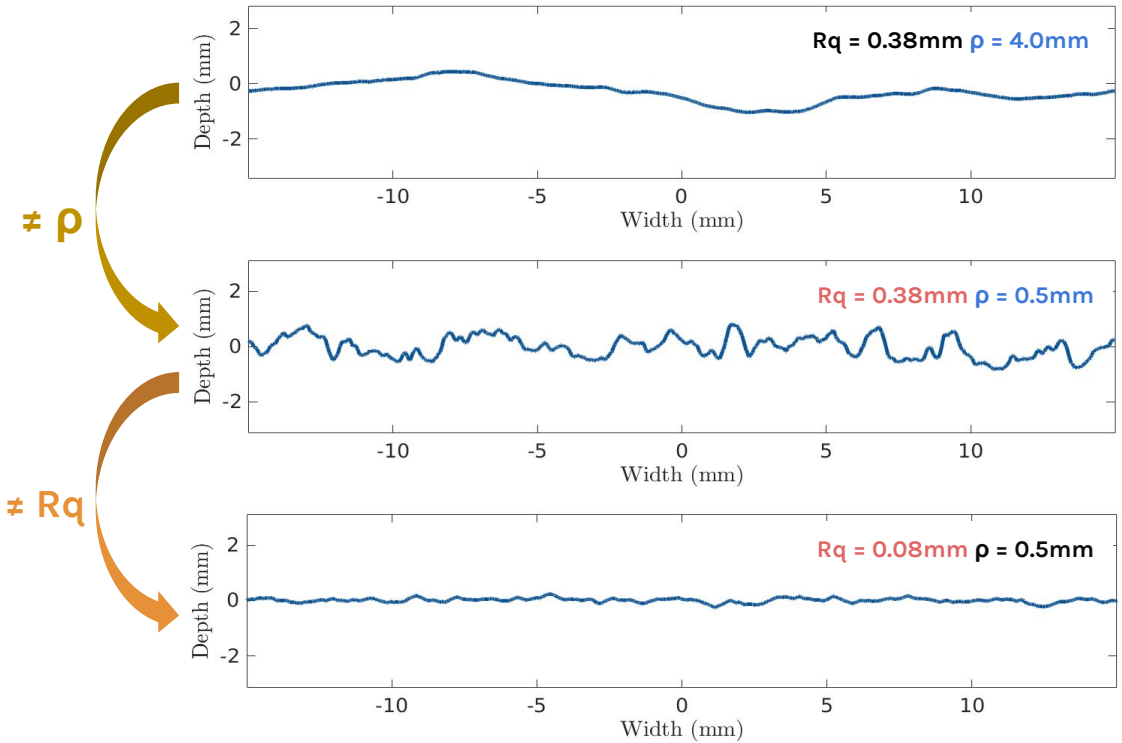

Fig 19 - Profile of height with differents parameters

Two parameters to describe the endosteum :

The **correlation length** ρ_{length}
⇒ distance over which the **autocorrelation function** of surface heights **is equal to 1/e**

ρ_{length} ↘ ⇒ More rough

The **height root mean square Rq**
⇒ average of **height variations** relative to a smooth surface

Rq ↗ ⇒ More rough

Bone microstructure characterization

The porosity of the bone

wavelength in the bone : ~ mm
⇒ Resolution : ~ mm
⇒ Object **smaller than a few mm** can **not be distinguished**

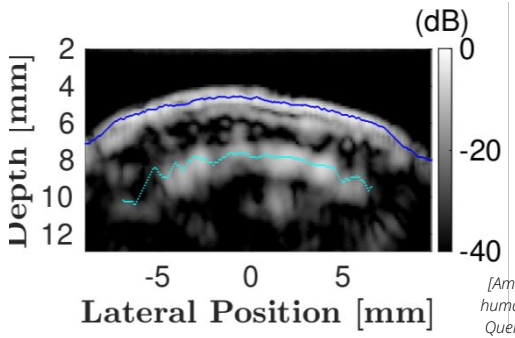

Fig 20 - Resolution of the specular beamformed image

[Amadou Dia. "Quantitative ultrasound imaging of human cortical bone". Thèse de doctorat dirigée par Quentin GRIMAL et Guillaume RENAUD. PhD thesis. 2024, 1 vol. (167 p.)]

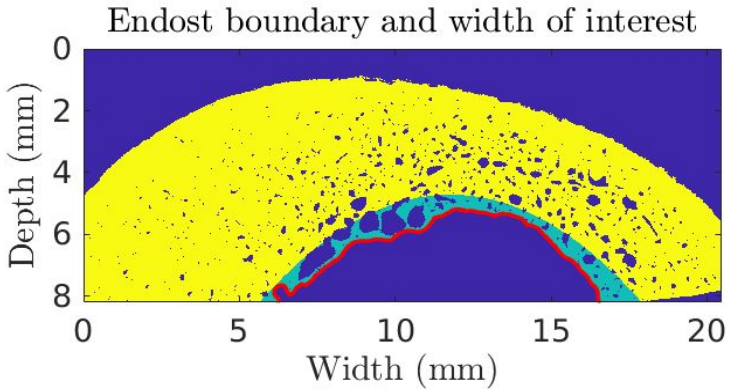

Fig 21 - Zone of Interest above the boundary

— Endosteal boundary
one wavelength around the boundary

Pore behind the interface confused with the interface

Porosity at the endosteal boundary **E.Pore = Volume of Pore / Total Volume**
Diameter of the pore in the endosteal boundary **d.Pore**

LIB16
Laboratoire d'Imagerie Biomédicale

Bone microstructure characterization

Conclusion on the parameters of characterisation of the bone

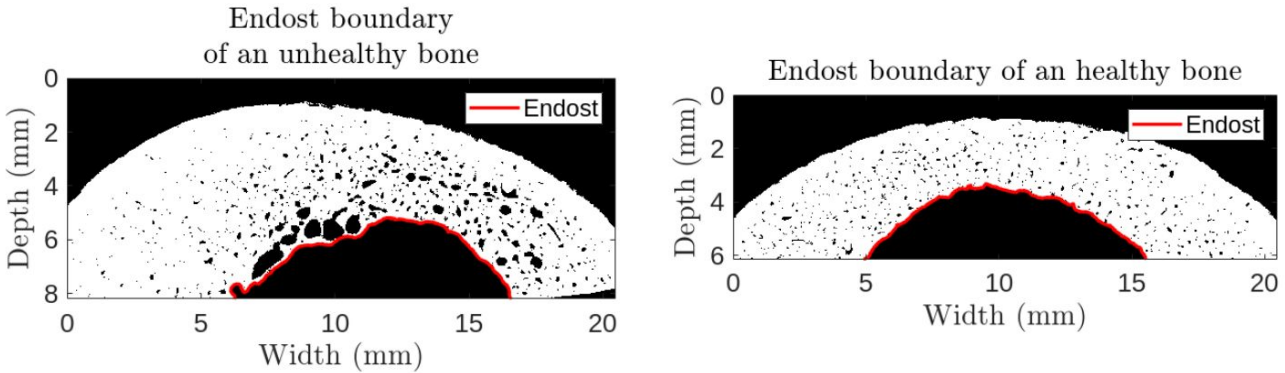

Fig 22 - Healthy (left) and unhealthy (right) bones

height RMS	Rq = 0.20 mm	>	Rq = 0.16 mm
Correlation length	ρ = 1.240 mm	<	ρ = 2.040 mm
Porosity near the endost	E.Pore = 32.3 %	>	E.Pore = 5.3 %
Diameter near the endost	d.Pore = 0.41 mm	>	d.Pore = 0.13 mm

Those parameters allows us to discern bones with different microstructures

Generation of surfaces

Generation of surfaces following **statistical laws** with **different parameters**

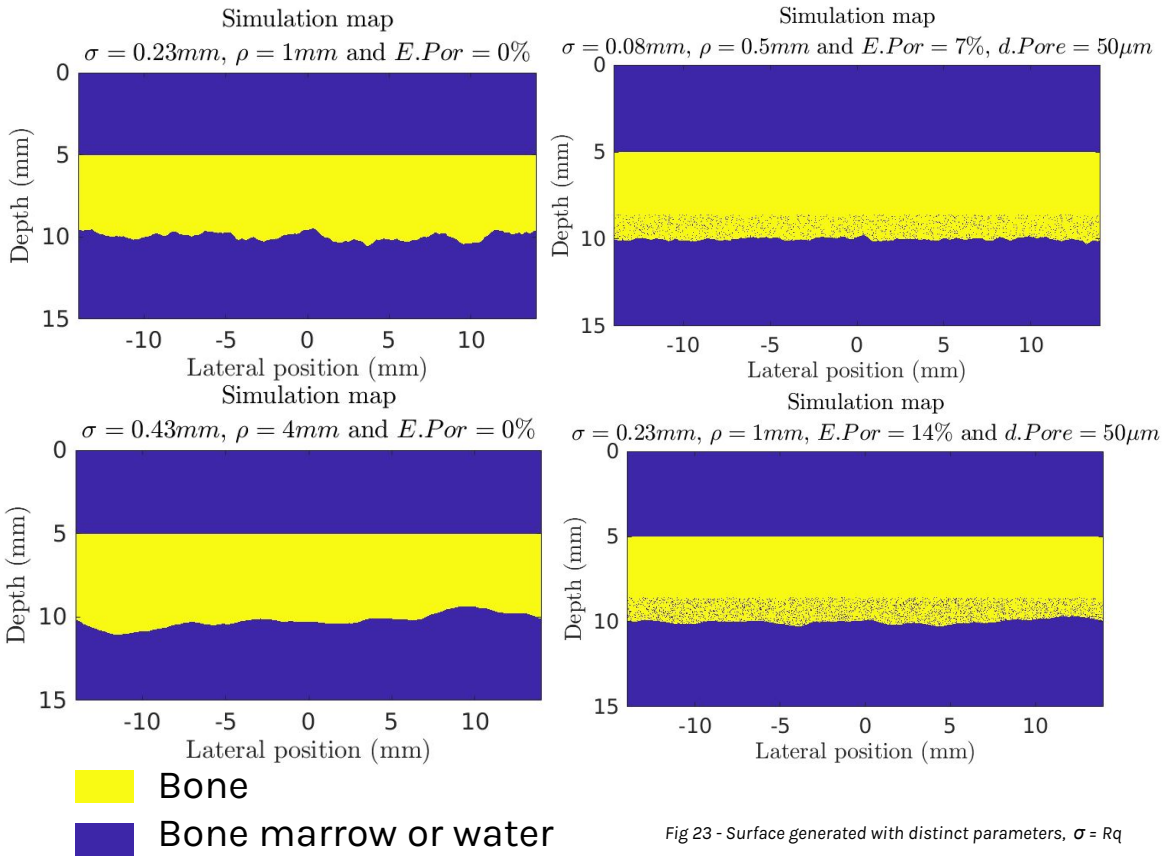

Fig 23 - Surface generated with distinct parameters, σ = Rq

1. Generation of surface :

a. Normal height distribution, with the standard deviation = Rq

b. Gaussian filter to obtain the desired ρ_{length}

2. Insertion of pores

a. Iterative addition of pore until E.Pore is reached

b. d.Pore is constant for each simulation

Comportement of the specular index regarding the parameters of characterisation

Simulation on SIMSONIC

SIMSONIC – Simulate the imaging sequences :

emission
propagation in the medium
reception

} of the **ultrasounds waves**

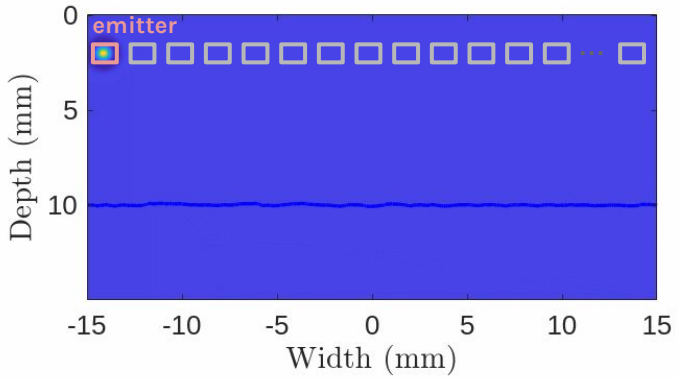

Fig 24 - Propagation of ultrasonic wave and interaction with an interface with Rq = 0.38 mm and ρ = 0.5mm

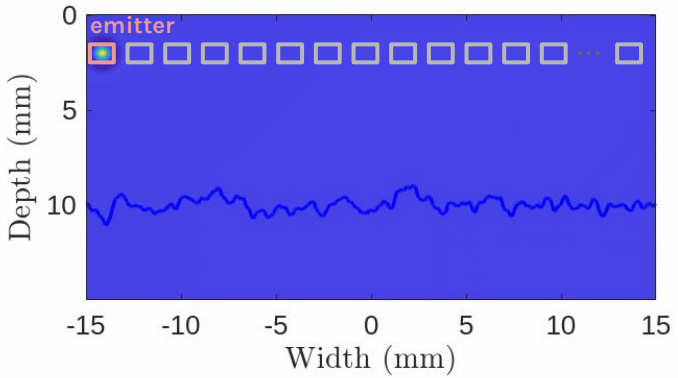

Fig 25 - Propagation of ultrasonic wave and interaction with an interface with Rq = 0.03 mm and ρ = 0.5mm

Comportement of the specular index regarding the parameters of characterisation

Post-process of the data

→ Computation of the **specularity index**

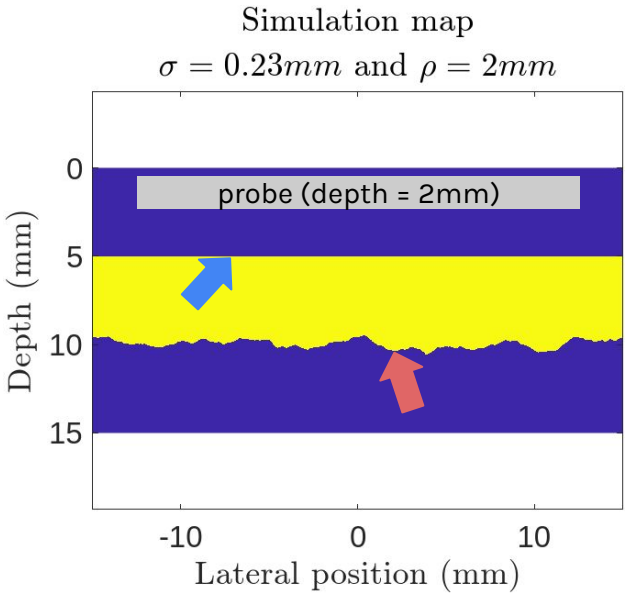

Fig 26 - Surface generated with Rq = 0.23mm and ρ = 2mm

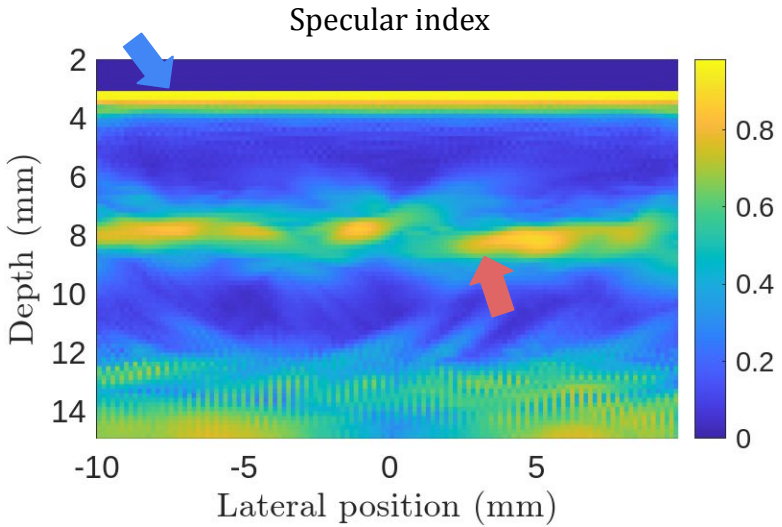

Fig 27 - Corresponding specularity map

LIB20
Laboratoire d'Imagerie Biomédicale

Comportement of the specular index regarding the parameters of characterisation

post-process of the data

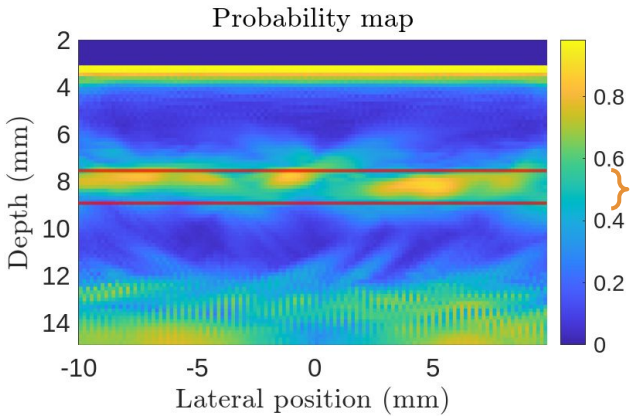

Fig 28 - Corresponding specularity map

Region Of Interest (ROI)

Metrics of analysis

- mean lateral specular index in the ROI
- mean specular index in the ROI

Since the variance of the lateral specular index is smaller than 3% for all the simulations, only the mean specular index in the ROI will be studied

Comportement of the specular index regarding the parameters of characterisation

Conclusions on the results

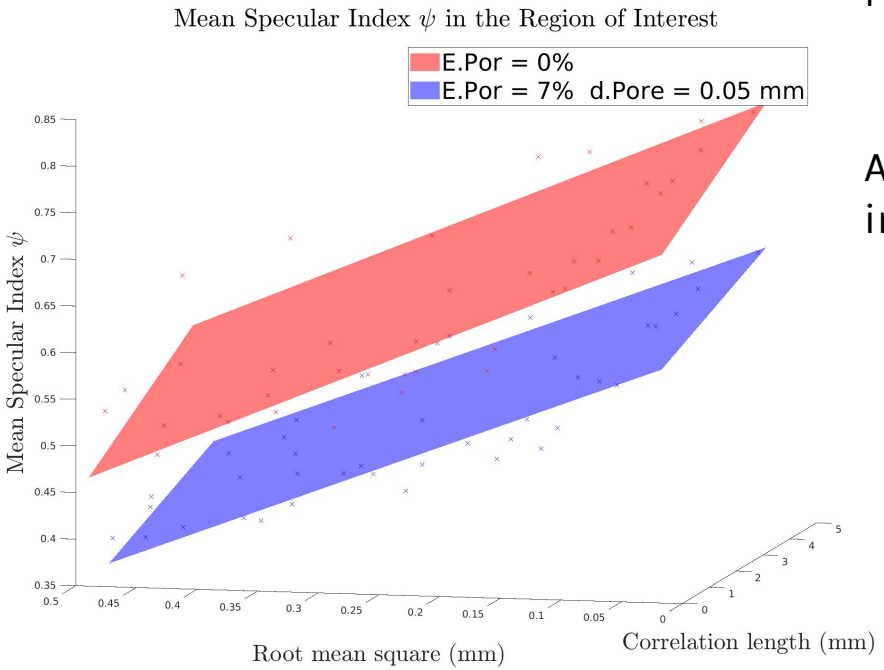

Fig 29 - Results of the simulations

Formula of the plan for a porosity of E.Por = 0% :

$$\overline{\psi_{\text{S.ROI}}} = -0.54 * Rq + 0.02 * \rho_{\text{length}} + 0.72$$

A porosity of 7% reduces the mean specular index in the ROI of almost 20%

The **height root mean square Rq** and the **porosity** have high influence on the mean specularity

Comportement of the specular index regarding the parameters of characterisation

Conclusions on the results

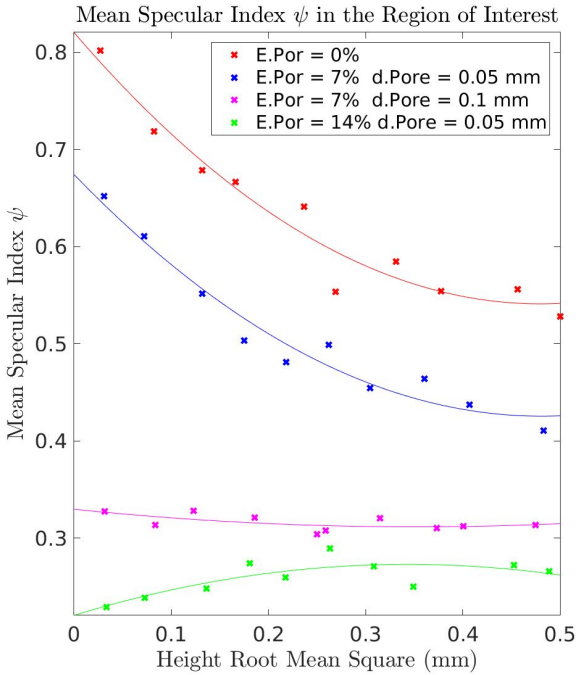

Fig 30 - Results of the simulations including porosity and diameter of the pores

Increases of the size of pores

⇒ Specular reflexion on the pore

⇒ Endosteal not detected

Increases of porosity up to 14%

⇒ Pores too concentrated at the endost

⇒ Endosteal not detected

Study of the **limits of endosteal detection** regarding the **pores parameters**

LIB23
Laboratoire d'Imagerie Biomédicale

Methodology of the research

How does the specular index Ψ behave regarding the bone microstructure ?

The height root mean square **Rq**, the correlation length $\boldsymbol{\rho_{length}}$, the porosity at the endost **E.Pore** and the pore diameter **d.Pore** **describe the bone interface**

The height root mean square **Rq,** the porosity at the endost **E.Pore** and the pore diameter **d.Pore** are highly **influencing the mean specularity** near the endost

LIB24
Laboratoire d'Imagerie Biomédicale

Perspectives for the end of the internship

Simulate on *ex-vivo* bones imaging

Compare the results with experimental results on *ex-vivo* bone

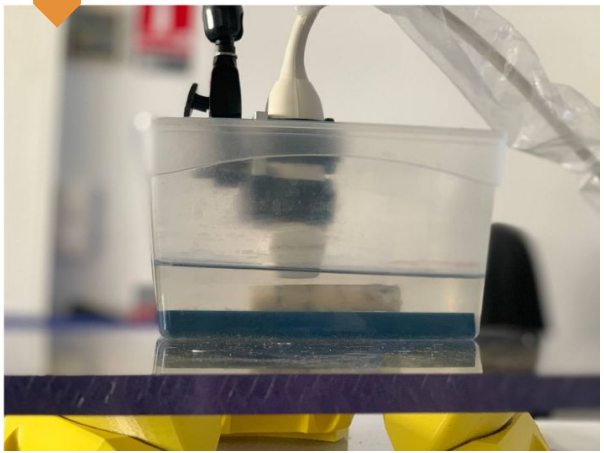

Fig 33 - Experimental setup for ultrasound acquisitions

[Amadou Dia. "Quantitative ultrasound imaging of human cortical bone". Thèse de doctorat dirigée par Quentin GRIMAL et Guillaume RENAUD. PhD thesis. 2024, 1 vol. (167 p.)]

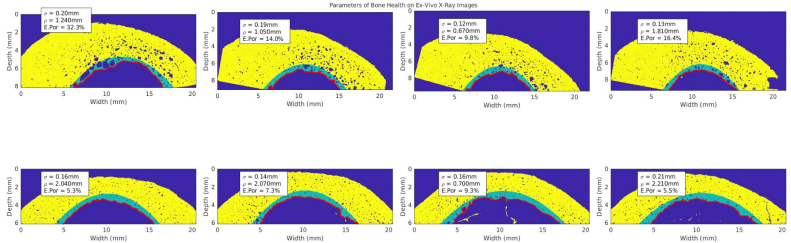

Fig 31 - Simulations on Ex-Vivo images

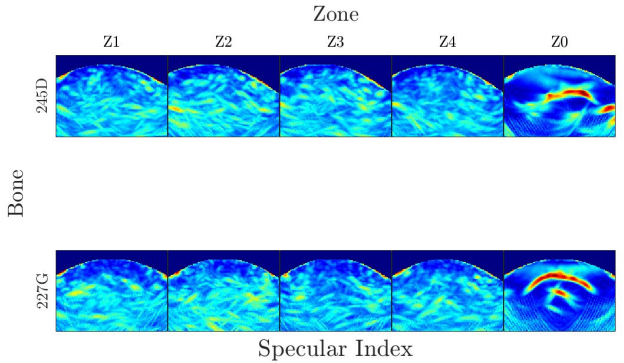

Fig 32 - Specular index on simulated ex-vivo bones

LIB25
Laboratoire d'Imagerie Biomédicale

Perspective for the diagnosis of osteoporosis

The medical context

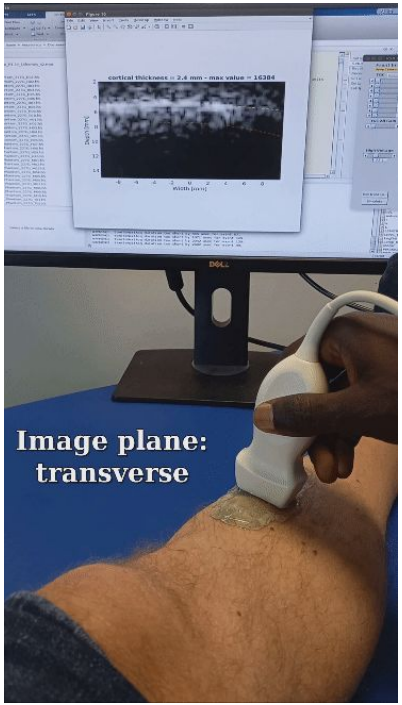

Fig 34 - Setup for ultrasound acquisitions

If we observe a **trend**, a **tendency**

➡ Trial on larger set of ex-vivo bones

➡ Trial on healthy voluntaries

➡ Clinical trial

Diagnosis: ultrasound imaging of the bone

➡ The ***bone thickness***, the ***density*** (or porosity) as well as the ***roughness*** is shown.

➡ ***Colored endosteum*** regarding the ***degree of porosity***

Thank you

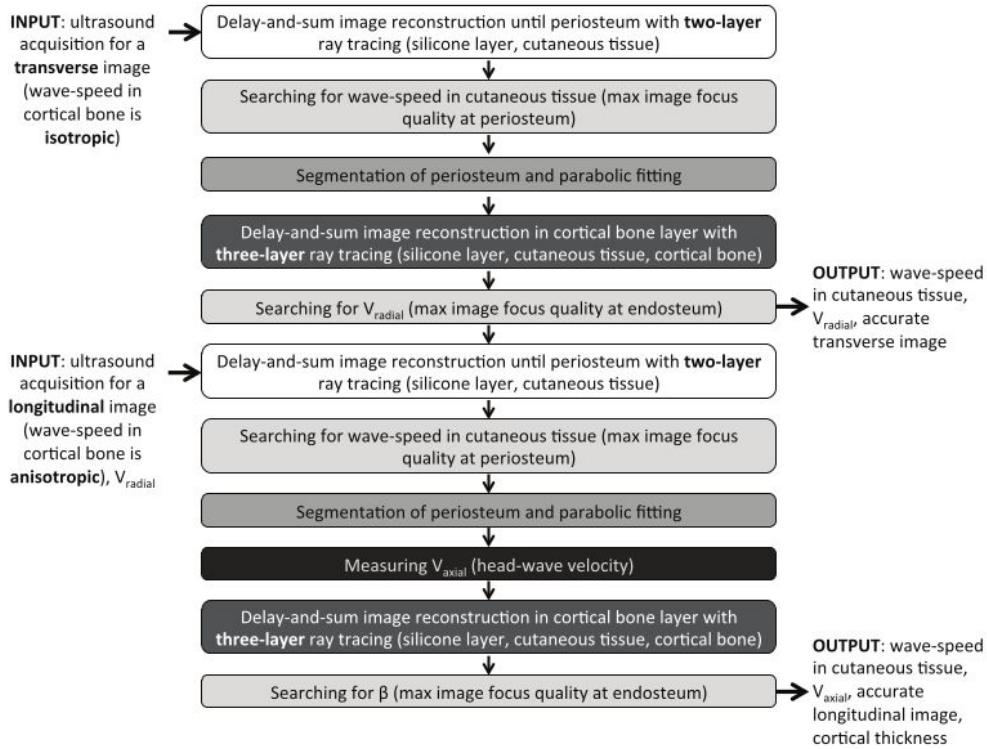

Figure 4. Graphical overview of the methodology. Steps applying the same processing are displayed with the same shade of gray.